Ground state of Ho atoms on Pt(111) metal surfaces: Implications for magnetism

M. Karbowiak[1,*] and C. Rudowicz[2,†]
[1]*Faculty of Chemistry, University of Wrocław, ul. F. Joliot-Curie 14, 50-383 Wrocław, Poland*
[2]*Faculty of Chemistry, A. Mickiewicz University, Umultowska 89B, 61-614 Poznań, Poland*
(Received 24 February 2016; published 16 May 2016)

We investigated the ground state of Ho atoms adsorbed on the Pt(111) surface, for which conflicting results exist. The density functional theory (DFT) calculations yielded the Ho ground state as $|J_z = \pm 8\rangle$. Interpretation of x-ray absorption spectroscopy and x-ray magnetic circular dichroism spectra and the magnetization curves indicated the ground state as $|J_z = \pm 6\rangle$. Superposition model is employed to predict the crystal-field (CF) parameters based on the structural data for the system Ho/Pt(111) obtained from the DFT modeling. Simultaneous diagonalization of the free-ion ($H_{\rm FI}$) and the trigonal CF Hamiltonian ($H_{\rm CF}$) within the whole configuration $4f^{10}$ of Ho^{3+} ion was performed. The role of the trigonal CF terms, neglected in the pure uniaxial CF model used previously for interpretation of experimental spectra, is found significant, whereas the sixth-rank CF terms may be neglected in agreement with the DFT predictions. The results provide substantial support for the experimental designation of the $|J_z = \pm 6\rangle$ ground state, albeit with subtle difference due to admixture of other $|J_z\rangle$ states, but run against the DFT-based designation of the $|J_z = \pm 8\rangle$ ground state. A subtle splitting of the ground energy level with the state (predominantly), $|J_z = \pm 6\rangle$ is predicted. This paper provides better insight into the single-ion magnetic behavior of the Ho/Pt(111) system by helping to resolve the controversy concerning the Ho ground state. Experimental techniques with greater resolution powers are suggested for direct confirmation of this splitting and C_{3v} symmetry experienced by the Ho atom.

DOI: 10.1103/PhysRevB.93.184415

I. INTRODUCTION

The study of individual magnetic atoms adsorbed on surfaces, i.e. adatoms, is a rapidly developing area of molecular magnetism [1–5]. Both transition-metal ions, e.g. Fe^{2+} [6,7] and Mn^{3+} [8], and rare-earth (RE) ions, e.g. Ho^{3+}, Er^{3+} [9,10], on various surfaces have been studied both experimentally using x-ray absorption spectroscopy (XAS), magnetic dichroism, and scanning tunneling microscopy (STM), as well as theoretically using semiempirical and *ab initio* methods. The driving motivation in studies of single atoms adsorbed on a solid surface [1–10] is the ultimate reduction of the size limit of nanoscale quantum magnets, since magnetic adatoms may serve as memory bits [11]. Semiempirical methods [6–10] are particularly useful since symmetry effects play an important role on the spin switching of adatoms [12,13]. The underlying concepts encompass the physical Hamiltonians, which include the crystal-field (CF) Hamiltonians $H_{\rm CF}$, and the effective spin Hamiltonians (SHs) $\tilde{H}_{\rm eff} \equiv \tilde{H}_{\rm SH}$, that include two major terms: the zero-field splitting (ZFS) Hamiltonians $\tilde{H}_{\rm ZFS}$ and the Zeeman electronic (Ze) ones $\tilde{\rm H}_{\rm Ze}$. The physical free ion Hamiltonians together with $H_{\rm CF}$ are fundamental in optical spectroscopy [14–18], whereas the effective SH (ZFS) Hamiltonians are fundamental in electron magnetic resonance (EMR) spectroscopy [19–21] of transition ions in crystals or their clusters. Together with the notion of magnetic anisotropy (MA), ZFS Hamiltonians and CF ones are fundamental in magnetism of transition-metal and RE ions [22–24]. The interface between the physical (CF/LF) Hamiltonians and the effective (spin) Hamiltonians have recently been critically reviewed [25–27].

In this paper, we focus on the recent controversy concerning the conflicting results on the ground state of Ho atoms on Pt(111) metal surfaces [9,10]. Miyamachi *et al.* [9] inferred the $|J_z = \pm 8\rangle$ ground state from density functional theory (DFT) calculations. This finding should be treated with caution, keeping in mind the ambiguities inherent in DFT calculations [28,29]. In order to determine experimentally the Ho ground state and MA, Donati *et al.* [10] measured XAS and x-ray magnetic circular dichroism (XMCD) spectra, and magnetization curves, and obtained the $|J_z = \pm 6\rangle$ ground state. The simulated XAS and XMCD spectra based on this J_z value agree with the experimental ones. This outcome is also corroborated by comparison of experimental and calculated magnetization curves [10]. The sets of CF parameters (CFPs) assigned to Ho^{3+} ions [9,10] are critically reexamined.

Karlewski *et al.* [11] suggested, based on analysis of dependence of the relaxation times with applied voltage, that the CFP set [9] was more reliable. This set leads to long spin-life times, which agrees with the inelastic electron tunneling spectroscopy (IETS) results [9,30]. The observed spin-life times [10] are substantially shorter than those calculated by Karlewski *et al.* [11] and measured experimentally using IETS [9]. Recently, based on spin-polarized STM experiments and first-principles calculations Coffey *et al.* [31] have suggested that the $4f$ electrons do not contribute to the spin-polarized tunneling process in RE single atoms on metals. Hence, one shall not expect to observe an inelastic process related to the $4f$ shell, suggesting that the IETS spectra [9] might have a different origin, which supports the conclusions of the XAS and XMCD experiments of Donati *et al.* [10]. In view of the controversial results described above, we attempt to determine independently the ground state of Ho

*miroslaw.karbowiak@chem.uni.wroc.pl
†On leave of absence from: Modeling in Spectroscopy Group, Institute of Physics, West Pomeranian University of Technology Szczecin, Al. Piastów 17, 70-310 Szczecin, Poland.

atoms on Pt(111) metal surfaces and assess its implications for magnetism.

The organization of this paper is as follows. In Sec. II, the theoretical background for CF analysis and superposition model (SPM) calculations is outlined. Analysis of magnetization curves and determination of CFPs is carried out in Sec. III. Summary and conclusions are given in Sec. IV.

II. CF ANALYSIS AND SPM CALCULATIONS

The methodology is based on CF theory, which underlies semiempirical determination of the ground states [25]. For the CF [or equivalently ligand field (LF)] analysis [25,32], we utilize the Reid's program [33,34], which incorporates the Hamiltonian $\hat{H} = \hat{H}_{\rm FI} + \hat{H}_{\rm CF}$, acting within the full $4f^{\rm N}$ configuration, and enables simultaneous diagonalization of the two parts – the free-ion ($\hat{H}_{\rm FI}$) Hamiltonian

$$\hat{H}_{\rm FI} = E_{\rm ave} + \sum_{k=2,4,6} F^k(nf,nf)\hat{f}_k + \zeta_{4f}\hat{A}_{\rm SO} + \alpha\hat{L}(\hat{L}+1) + \beta\hat{G}(G_2) + \gamma\hat{G}(R_7) + \sum_{i=2,3,4,6,7,8} T^i\hat{t}_i + \sum_{j=0,2,4} M^j\hat{m}_j + \sum_{k=2,4,6} P^k\hat{p}_k, \quad (1)$$

and the CF Hamiltonian expressed in the Wybourne notation [17] in the compact form [35]

$$\hat{H}_{\rm CF} = \sum_{k,q} B_{kq}\hat{C}^{(k)}_q(x,y,z). \quad (2)$$

The operators and interaction parameters in Eq. (1) as well as the intraconfigurational spherical-tensor operators $\hat{C}^{(k)}_q$, expressed in a given axis system (x, y, z), and the symbolic CFPs B_{kq}, of rank k and component q, in Eq. (2) are defined according to the prevailing conventions; for details and references, see [32]. In low symmetry CFP studies of the transition-metal (TM) $3d^{\rm N}$ ions and the RE $4f^{\rm N}$ ions in crystals, the expanded form is most often used, in which the Re and Im parts of the complex CFPs in Eq. (2) are explicitly indicated: $B_{kq} = {\rm Re}B_{kq} + i{\rm Im}B_{kq}$. Due to properties of the Wybourne operators [17] $B_{k-q} = (-1)^q B^*_{kq}$ (see, e.g. Refs. [25] and [36]), the relations hold: ${\rm Re}B_{k-q} = (-1)^q {\rm Re}B_{kq}$, ${\rm Im}B_{k-q} = (-1)^{q+1}{\rm Im}B_{kq}$. The disparate forms of $\hat{H}_{\rm CF}$ expressed in the Wybourne notation, both compact and expanded ones, identified in literature have been critically reviewed [37].

The SPM [14–16] is employed along the lines described in Refs. [38] and [39]. Based on the knowledge of the structural data for Ho atoms on Pt(111) surfaces provided in the Supplemental Material [40], the CFPs used in our analysis are estimated using SPM. The usefulness of SPM in analysis of CF effects in RE ion based intermetallic compounds has been proven, e.g. in Refs. [41] and [42]. The SPM expressions for CFPs defined in Eq. (2) are (for details and references, see [32,38,39])

$$\begin{aligned} {\rm Re}B_{kq} &= \sum_L \bar{B}_k(R_L) g_{k,q}(\theta_L,\phi_L), \\ {\rm Im}B_{kq} &= \sum_L \bar{B}_k(R_L) g_{k,-q}(\theta_L,\phi_L), \end{aligned} \quad (3)$$

where $\bar{B}_k$ are the intrinsic parameters, and $g_{k,q}$ are the coordination factors. The listing of the coordination factors expressed in the (extended) Stevens operator notation [43,44] may be found in Ref. [45], but in the Wybourne one in Refs. [14,46]. In the SPM model, the distance dependence is assumed in the form of a power law with the coefficients t_k [14,46]

$$\bar{B}_k(R) = \bar{B}_k(R_0)(R_0/R)^{t_k}, \quad (4)$$

where R_0 is usually assumed to be the average metal-ligand distance. Equation (4) may be than rewritten as

$$\begin{aligned} {\rm Re}B_{kq} &= \sum_L \bar{B}_k(R_0)(R_0/R_L)^{t_k} g_{k,q}(\theta_L,\phi_L), \\ {\rm Im}B_{kq} &= \sum_L \bar{B}_k(R_0)(R_0/R_L)^{t_k} g_{k,-q}(\theta_L,\phi_L). \end{aligned} \quad (5)$$

Since the structural data, which are indispensable as input for SPM/CFP analysis, have been obtained for the Ho/Pt(111) system [9], calculations are carried out for this case. The crystalline structure was determined [9] by DFT methods with the Vienna *Ab initio* Simulation Package (VASP). The DFT results indicate that the Ho atoms in the face-centered-cubic (fcc) and hexagonal close-packed (hcp) positions are located 0.213 and 0.214 nm, respectively, above the Pt(111) surface. The spherical polar coordinates (R, θ, φ) of Pt atoms in the nearest vicinity of Ho atoms at the hcp sites are listed in Table SI [40], whereas the Cartesian axis system adopted for SPM calculations together with its orientation with respect to the Cartesian crystallographic axis system [CAS] (a, b, c) are depicted in Fig. S1 [40].

The nearest surrounding of Ho^{3+} ions is formed by three Pt atoms in the first coordination sphere (at $R = 0.2695$ nm) and three Pt atoms in the second sphere (at $R = 0.3892$ nm); all atoms belong to the same layer. The next nearest Pt atom (at $R = 0.4446$ nm) belongs to the second layer and is located in the hcp site below a given Ho atom. The atomic coordinates of Ho atoms in the fcc sites are identical to those in the hcp sites, whereas the only difference between the two sites is that no Pt ($x, y = 0.0$) atom is located in the second layer in the fcc sites. The local site symmetry is C_{3v} in both sites. For these reasons, the SPM/CFP calculations presented below have been carried out for Ho^{3+} ions in the hcp sites. The coordination factors $g_{k,q}$ [32,38,39] calculated for Ho atoms at the hcp sites on the Pt(111) surface are listed in Table SII [40], including the contributions from Pt atoms in the first and second coordination sphere and Pt atom in the second layer (see, Table SI [40]).

Using the initial CFP values predicted using SPM [40], simultaneous diagonalization of the free-ion ($H_{\rm FI}$) and the trigonal CF Hamiltonian ($H_{\rm CF}$) within the basis of all states of the configuration $4f^{10}$ of Ho^{3+} ion, including a complete set of SLJ multiplets, was performed. The energy levels and the corresponding eigenvectors calculated using the Reid's program [33,34] are presented partially below and in more details in Ref. [40]. For simulations of magnetization and fitting the CFPs to the experimental magnetization curves [10], the more advanced and versatile CONDON program [47,48] has been utilized.

TABLE I. Trigonal CFP sets: original B_k^q, converted by us to B_{kq}, and obtained in the present analysis.

	Original [μeV]			Converted [cm^{-1}]		This
CFP	[9]	[10]	CFP	[9]	[10]	paper
B_0^2	-239	-140	B_{20}	1737	1017	1706
B_0^4	8.6×10^{-2}	1.06	B_{40}	-167	-2054	-2138
B_3^4	0.293	0	B_{43}	-24	0	1295
B_0^6	1.87×10^{-4}		B_{60}	-18.6		0
B_3^6	-1.97×10^{-3}		B_{63}	9.6		0
B_6^6	6.3×10^{-4}		B_{66}	-4.1		0

III. ANALYSIS OF MAGNETIZATION CURVES AND DETERMINATION OF CFPS

The energy levels and eigenvectors are calculated using simultaneous diagonalization of the free-ion Hamiltonian ($H_{\rm FI}$) and the trigonal $H_{\rm CF}$ in the Wybourne notation [17,25,37] within the $Ho^{3+}(4f^{10})$ configuration [40]. The CFP sets calculated by *ab initio* methods and the first-order perturbation theory for Ho atoms on Pt(111) in the fcc position (Table I in SI of [9]) and those determined by fitting the XAS and XMCD spectra and the magnetization curves to the simulated results based on ligand-field multiplet calculations (Table I in SI of [10]) are converted to the Wybourne notation (Table I). The CFPs B_k^q (in the Stevens notation [43,44]) pertain to a restricted $H_{\rm CF}$ [25] acting only within the Ho ground multiplet $^5I_8$ in [9] and a full $H_{\rm CF}$ acting on the complete multiplet set in Ref. [10].

The experimental analysis [10] included only the second-rank CF terms and a truncated form of the fourth-rank CF terms [40], but the theoretical analysis [9] included also the sixth-rank CF terms (Table I). Nevertheless, the latter CFPs are negligible as compared with the second- and fourth-rank CFPs. Both studies indicate the axial [10] or nearly axial [9] CF potential of markedly different magnitude (Table I), in the latter case dominated by the CFP B_0^2 (B_{20}). The major physical difference between the two approaches concerns the ground state of Ho atoms on Pt(111) metal surfaces determined as $|J_z = \pm 8\rangle$ [9] and $|J_z = \pm 6\rangle$ [10]. This leads to a serious controversy.

Donati *et al.* [10] employed the CFP set determined by them and that predicted by Miyamachi *et al.* [9] to simulate the magnetization versus applied magnetic field. The results [10] show that correct description of the experimental dependence cannot be achieved using the latter set. The simulations of magnetization using the CONDON program [47,48] indicate [40] that the experimental magnetization curves [10] are relatively well reproduced using the CFPs of Donati *et al.* [10] (Fig. 1) and thus corroborate their finding. However, a deeper analysis of Fig. 1 reveals that, for the normal incidence (0°) in the range of applied magnetic field 0.2–3 T, the calculated magnetization curve runs slightly above the experimental data points.

Using CONDON [47,48], we performed fittings of the data points read out from in Fig. 2 of Ref. [10] with two adjustable CFPs B_{20} and B_{40}; so-obtained magnetization curves are practically the same as in Ref. [10]. However,

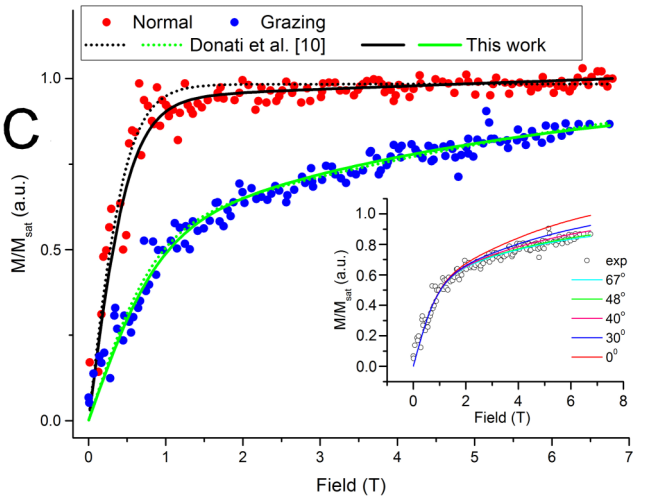

FIG. 1. Magnetization curves of Ho/Pt(111) versus applied magnetic field measured [10] for the normal (0°) and grazing (55°) incidence and the simulated curves (see text). For clarity, only the values for the applied magnetic field $\boldsymbol{B} > 0$ are shown. Inset presents magnetization curves of Ho/Pt(111) versus $\boldsymbol{B}$ calculated for the grazing incidence while varying the angle φ (see text).

the values of the coordination factors $g_{k,q}$ (Table SII [40]) suggest that, for Ho atoms at the hcp sites on the Pt(111) surface, the contribution to the CF potential from B_{43}(CFP) is not negligibly small. Assuming that the power law exponent t_4 is in the range 2–12 [40], the ratio B_{40}/B_{43} is obtained between -10.2 and -0.94. Hence, next fittings were carried out using $H_{\rm CF}$ including also B_{43}(CFP). At the initial stages B_{43}(CFP) was expressed by the fixed ratio with respect to B_{40}, determined from the SPM calculations using $g_{k,q}$ in Table SII [40] for various values of t_4 in the range 2–12. After preliminary determination of B_{43} (with best fitting obtained for $t_4 = 5.1$, corresponding to $B_{40}/B_{43} = -1.43$), the fine-tuning was carried out freeing simultaneously the CFPs: B_{20}, B_{40}, B_{43}. Parameters were fitted independently to the magnetization curves for the normal and grazing incidence using the experimental data in Fig. 2 of [10].

This procedure yielded B_{20}, B_{40}, and B_{43} (in cm^{-1}) as: 1741, -1954, and 1376 (set N) for the normal incidence, but 1671, -2328, and 1214 (set G) for the grazing incidence, respectively. In the two cases, the fitted B_{20} (B_{40}) is very close, both in sign and magnitude, whereas B_{43} differs somewhat but still acceptably. Such differences between CFP sets obtained from fitting data for the normal and grazing incidence may arise from varying quality of the experimental data points (their relatively large random distribution) or may indicate different accuracy of a given parameter determination. The magnetization curves of Ho/Pt(111) versus applied magnetic field calculated using these CFP values are depicted in Fig. 1. For the normal incidence, the simulated curve is markedly closer to the experimental data points [10] than the originally simulated curve [10], whereas for the grazing incidence, both curves are practically the same.

Subsequently, fittings were carried out using $H_{\rm CF}$ including also the sixth-rank CFPs to check their influence on quality of fittings. However, their effect is practically unnoticeable,

TABLE II. The lowest four energies, their expectation values $\langle J_z \rangle$ and eigenvectors calculated for the CFP set A.

Eigenstate	Energy (cm^{-1})	$\langle J_z \rangle$	Eigenvectors
$\Psi^s_{\pm 6}$	0.	0.	$0.6650\|+6\rangle(44.2\%) + 0.6650\|-6\rangle(44.2\%) - 0.2347\|+3\rangle(5.5\%) + 0.2347\|-3\rangle(5.5\%)$
$\Psi^a_{\pm 6}$	1.15	0.	$0.6684\|+6\rangle(44.7\%) - 0.6684\|-6\rangle(44.7\%) - 0.2277\|+3\rangle(5.2\%) - 0.2277\|-3\rangle > (5.2\%)$
Ψ_7	10.20	6.298	$0.8785\|+7\rangle(77.2\%) - 0.4668\|+4\rangle(21.8\%)$
Ψ_{-7}	10.20	−6.298	$0.8785\|-7\rangle(77.2\%) + 0.4668\|-4\rangle(21.8\%)$
Ψ_5	41.87	5.104	$0.9095\|+5\rangle(82.7\%) + 0.3205\|+8\rangle(10.3\%) - 0.2586\|+2\rangle(6.7\%)$
Ψ_{-5}	41.87	−5.104	$0.9095\|-5\rangle(82.7\%) + 0.3205\|-8\rangle(10.3\%) + 0.2586\|-2\rangle(6.7\%)$

since the simulated magnetization curves are exactly the same as using only the second- and fourth-rank CFPs. For the normal incidence, these fittings yielded CFPs B_{20}, B_{40}, B_{43}, B_{60}, B_{63}, and B_{66} (in cm^{-1}) as: 2174, −1656, 1012, 163, −167, and −22, respectively. The sixth-rank CFPs are small comparing with the second- and fourth-rank CFPs. Superposition model analysis of so-obtained sixth-rank CFPs (using $g_{k,q}$ in Table SII [40]) enables extracting the model parameters as $\bar{B}_6 = -132\,cm^{-1}$ and $t_6 = 10.8$. The $\bar{B}_6$ value agrees well with those reported for RE ions in intermetallic compounds [41,42], where generally, the intrinsic parameter $\bar{B}_6$ attains rather small and negative values. For example, for HoX (where X = Rh, Cu, Ag, or Zn), the values of $\bar{B}_6$ in the range (−77)–(−112) cm^{-1} were obtained [41], but for $Ho_{0.05}Y_{0.95}Pd_3$, $\bar{B}_6 = -1.6\,cm^{-1}$ [42]. For the grazing incidence, these fittings could not provide sensible values of the sixth-rank CFPs consistent with those obtained for the normal incidence. The reason may be that the magnetization curves for each incidence are insensitive to the B_{6q} changes. Nevertheless, small B_{6q} values may be expected also for the grazing incidence. Attempts to include B_{6q}'s in fittings, when freeing them simultaneously with B_{2q}'s and B_{4q}'s, may result in less reliable values of the latter CFPs. Hence, subsequent discussion is restricted to the results (set N and G) obtained from fittings carried out using only B_{2q}'s and B_{4q}'s as adjustable parameters. As the final set A, we consider the average values of B_{20}, B_{40}, and B_{43} from the sets N and G (in cm^{-1}): 1706, −2138, and 1295.

Analysis of so-obtained CFP set A in terms of SPM (using $g_{k,q}$ in Table SII [40]) enables extracting the model parameters for Ho atoms in the hcp position on the Pt(111) surface as $\bar{B}_4 = 2681\,cm^{-1}$ and $t_4 = 4.4$. Assuming Ho atoms in the fcc position, which lacks only the Pt(second layer), we obtain $B_4 = 2450\,cm^{-1}$ and $t_4 = 4.9$. The t_4 values agree reasonably well with those used in earlier SPM analyses for RE ions in intermetallic compounds [41,42]. This comparison indicates that SPM [14–16,38,39] is capable of yielding reliable results also for magnetic atoms adsorbed on surfaces.

Having confirmed applicability of SPM for adatoms based on the results of Ref. [10], similar SPM analysis is carried out for the DFT-obtained CFPs [9]. So-extracted model parameters are $\bar{B}_4 = 198\,cm^{-1}$ and $t_4 = 1.3$ for the Ho atoms in the hcp position on the Pt(111) surface, but $\bar{B}_4 = 116\,cm^{-1}$ and $t_4 = 1.0$ for the fcc position. The t_4 values seem to be too small as compared with those expected for RE ions in intermetallic compounds [41,42], whereas completely unphysical t_6 values are obtained: $t_6 = 53.2$ (hcp) and $t_6 = 56.7$ (fcc). These findings, together with observation that the CFPs [9] do not reproduce satisfactorily magnetization curves for the grazing incidence [10], indicate that the CFPs [9] are not reliable.

Analysis [10] of the magnetization curves obtained at 0° (normal incidence) and 55° (grazing incidence) for Ho/Pt(111) took into account only the axial CFPs B_{20} and B_{40}. So-calculated magnetization curve depends on the angle θ between the magnetization vector and the axis perpendicular to the Pt(111) surface, however, is independent of the angle φ between the x axis and the projection of the magnetization vector on the x-y plane. Including in H_{CF} the terms B_3^4 (B_{43}) induces dependence of the magnetization curves calculated for the grazing incidence on the angle φ. The magnetization curves of Ho/Pt(111) versus applied magnetic field, calculated for the grazing incidence using various angles φ, are depicted in Fig. 1 (inset). These calculations indicate the best agreement of the simulated and experimental curves for $\varphi = 48°$; the value of φ, for which the experimental magnetization curve was determined [10] was not indicated therein.

Eigenvectors calculated for the final CFP set A are given partially in Table II, but in full in Table SV [40]. The corresponding energy splittings and expectation values $\langle J_z \rangle$ of the quantum levels of a Ho atom on Pt(111) are depicted in Fig. 2. The major finding arising from these calculations is confirmation of the conclusion of Donati *et al.* [10] concerning the ground state of Ho atoms on Pt(111) metal surfaces. It

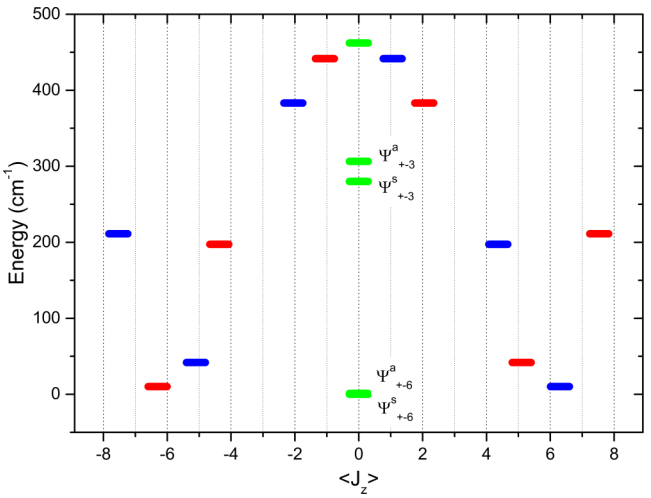

FIG. 2. The energy splittings of the quantum levels of a Ho atom on Pt(111) calculated for the CFP set A. The states mixed by the off-diagonal CF term (B_{43}) are indicated by the same color.

turns out that the designation of the ground state as $|J_z = \pm 6\rangle$, obtained based on interpretation of XAS and XMCD spectra and the magnetization curves [10] is well justified theoretically by semiempirical methods, including SPM and CF analysis. At the same time, the ground state $|J_z = \pm 8\rangle$ proposed by Miyamachi *et al.* [9] appears to contradict the results of present SPM and CF analysis.

The results in Table II and Fig. 2 enable considering implications for magnetism. Donati *et al.* [10] interpreted XAS and XMCD spectra and the magnetization curves assuming purely uniaxial CF [49]. Hence, pure states $|J_z = \pm X\rangle$ were obtained [10], including the pure ground state $|J_z = \pm 6\rangle$. The present inclusion of B_{43} induces mixing of pure states differing by $\Delta J_z = \pm 3$, yielding the ground state arising predominantly from the states $|J_z = \pm 6\rangle$ with admixture of other states (see the percentage states composition in Table II and Table SV [40]). This leads to appearance of states with completely quenched angular momentum J_z. So-obtained ground state is a pseudodoublet $\Psi^a_{\pm 6}$ and $\Psi^s_{\pm 6}$ split in energy by $1.15\,\mathrm{cm}^{-1}$. Donati *et al.* [10] suggested the possibility of such mixing by showing in their Fig. 3 the states that may be mixed by B_{43}. However, for Ho/Pt(111), they provided only the fitted CFPs B_{20} and B_{40} and mentioned that simulations including $B_{43} = \pm 5\,\mu$eV yielded the results very close to those obtained with $B_{43} = 0$. Present calculations confirm that, if such small $B_{43} \sim 0.04\,\mathrm{cm}^{-1}$ is adopted, its effect is negligible; however, the much larger B_{43} value we derived significantly affects magnetization curves. The authors [10] also state: "The resulting $J_z = \pm 6$ ground state is particularly delicate since it can be mixed by the O_4^3 operators, consequently allowing quantum tunneling of the magnetization." Therefore, based on their experimentally determined ground state, as well as the energies and mixing of the quantum states, they do not expect large spin relaxation times for Ho/Pt(111) at $B = 0\,\mathrm{T}$. Such expectation of short spin relaxation times corroborates the experimental results [10] but contradicts those of Ref. [9].

Analysis of the excited states allows for the following conclusions. Assuming uniaxial CF [10], the first excited state was obtained as the pure state $|J_z = \pm 5\rangle$ at energy $31.7\,\mathrm{cm}^{-1}$, but the next excited state $|J_z = \pm 7\rangle$ at $44\,\mathrm{cm}^{-1}$. Including $B_3^4 = 5\,\mu$eV yields the first excited $\langle J_z\rangle = \pm 4.9826$ state at $31.25\,\mathrm{cm}^{-1}$, but the next excited $\langle J_z\rangle = \pm 6.6189$ state at $39.31\,\mathrm{cm}^{-1}$. These calculations yield, apart from mixed composition, a different sequence of the levels associated with the state (predominantly) $|J_z = \pm 7\rangle$ lying closer to the ground state at $10.20\,\mathrm{cm}^{-1}$, but the state (predominantly) $|J_z = \pm 5\rangle$ lying higher at $41.87\,\mathrm{cm}^{-1}$ (Table II). Hence, the present results generally support the corresponding results obtained by Donati *et al.* [10] but contradict those of Miyamachi *et al.* [9]. However, one important aspect revealed by SPM analysis concerns the validity of the purely uniaxial CF model adopted in Ref. [10]. Based on the predictions of group theory [50] as well as the relative magnitude of CF terms discussed in Ref. [40], the neglect of the nonaxial CFPs inherent in this model is deemed as unjustified. Hence, in view of these arguments, the purely uniaxial CF model can be considered only as a crude approximation [40], whereas more reliable results may be obtained when the CFP B_{43} is included in the CF calculations.

IV. SUMMARY AND CONCLUSIONS

In summary, the present results shed light on the structure of the energy levels and eigenvectors of Ho atoms on Pt(111) metal surfaces and have important bearing on explanation of their magnetic behavior. The semiempirical SPM analysis was carried out using the CF Hamiltonian including also the trigonal CFP B_{43}, unlike that of Donati *et al.* [10], where B_{43} was practically neglected in the final analysis of experimental results. Analysis of results [40] indicates that the contribution of B_{43} is comparable to that of B_{40}, and hence, the former parameter should not be ignored. The CFP B_{43} strongly affects the composition of the eigenvectors yielding the ground state arising predominantly from the states $|J_z = \pm 6\rangle$, as approximately determined experimentally [10], however, with significant admixture of other $|J_z\rangle$ states. Due to relatively high B_{43} value, the ground energy level with the pseudodoublet formed by the symmetric $\Psi^s_{\pm 6}$ and antisymmetric $\Psi^a_{\pm 6}$ states splits by $1.15\,\mathrm{cm}^{-1}$. Since this splitting is smaller than thermal energy at 2.5 K, the states $\Psi^s_{\pm 6}$ and $\Psi^a_{\pm 6}$ can be effectively coupled through transverse interaction even at low temperature. This may activate a magnetization reversal process via quantum tunneling, leading to significant shortening of spin relaxation time.

The major advantage offered by semiempirical SPM analysis of CFPs is resolving the controversy concerning the ground state of Ho atoms on Pt(111) metal surfaces. The results add substantial support for the designation made experimentally by Donati *et al.* [10] as basically $|J_z = \pm 6\rangle$, albeit with subtle difference due to admixture of other $|J_z\rangle$ states, but run against the designation based on the DFT calculations made by Miyamachi *et al.* [9] as $|J_z = \pm 8\rangle$. A very recent experimental study on Ho adatoms on Pt(111) brought to our attention during the referring process [51] corroborates our findings and thus contributes significantly to the solution of the controversy in question. When two independent studies indicate that the designation of the ground state of Ho atoms on Pt(111) metal surfaces as $|J_z = \pm 8\rangle$ [9] is rather unreliable, a question arises about what was forgotten or overestimated in the DFT calculations [9]. While no clear-cut answer to this question may be provided at this stage, one may only presume that, in view of the ambiguities inherent in methodology and interpretation of the DFT results, which strongly depend on the chosen basis of states and specific DFT software packages utilized [28,29], the DFT results [9] may need some reinterpretation. Importantly, such reinterpretation may follow the Coffey *et al.* [31] suggestion that the effects observed in the IETS spectra [9] might have a different origin since most probably the inelastic spin-polarized tunneling processes in single $4f$ shell atoms on metals are not due to the inner $4f$ shell electrons.

A crucial unsolved question is the applicability of the pure uniaxial CF model, which in our opinion is not well justified in the present case. It seems to us that such a model has been previously used in literature rather for numerical convenience to simplify the calculations rather than being based on solid physical grounds. The observed importance of the off-diagonal CF term $B_{43}C_3^{(4)}$ [40] revealed by SPM/CFP analysis may suggest further experiments to verify the actual symmetry of CF experienced by Ho atoms at the Pt(111) surface and

possible quenching of angular momentum J_z due to mixing of states differing by $\Delta J_z = \pm 3$ or ± 6. If the CF experienced by Ho atoms at the hcp and/or fcc sites has really C_{3v} symmetry, than one should observe experimentally a dependence of the magnetization curves measured for the grazing incidence on the angle φ. However, for the purely uniaxial CF, which could arise due to interaction of Ho atoms/ions with the electronic density delocalized at the Pt(111) surface, no such angle dependence should be observed. Discussion of feasibility of such experiments, which would require techniques with greater resolution powers, is beyond the scope of this paper.

Finally, we note [40] that aspects concerning the terminological confusions identified in adatoms-related literature will be surveyed in a separate review [52], whereas relationships between crucial notions have recently been investigated [53]; for details, see [40].

ACKNOWLEDGMENTS

The authors are grateful to Prof. Wulf Wulfhekel and Dr. Arthur Ernst for providing the VASP calculated data on the atomic positions of the Ho ions on the Pt(111) surface studied. One of us (CZR) is grateful to Dr. Marta Prada for useful discussions. Thanks are due to the anonymous reviewers for helpful comments and bringing a pertinent reference to our attention.

[1] H. Brune and P. Gambardella, Surf. Sci. **603**, 1812 (2009).
[2] J. P. Gauyacq, N. Lorente, and F. D. Novaes, Prog. Surf. Sci. **87**, 63 (2012).
[3] A. Caneschi, D. Gatteschi, and F. Totti, Coord. Chem. Rev. **289-290**, 357 (2015).
[4] T. Schuh, T. Balashov, T. Miyamachi, S. Wu, C. Kuo, A. Ernst, J. Henk, and W. Wulfhekel, Phys. Rev. B **84**, 104401 (2011).
[5] T. Schuh, T. Miyamachi, S. Gerstl, M. Geilhufe, M. Hoffmann, S. Ostanin, W. Hergert, A. Ernst, and W. Wulfhekel, Nano Lett. **12**, 4805 (2012).
[6] B. Bryant, A. Spinelli, J. J. T. Wagenaar, M. Gerrits, and A. F. Otte, Phys. Rev. Lett. **111**, 127203 (2013).
[7] M. Etzkorn, C. F. Hirjibehedin, A. Lehnert, S. Ouazi, S. Rusponi, S. Stepanow, P. Gambardella, C. Tieg, P. Thakur, A. I. Lichtenstein, A. B. Shick, S. Loth, A. J. Heinrich, and H. Brune, Phys. Rev. B **92**, 184406 (2015).
[8] C. F. Hirjibehedin, C.-Y. Lin, A. F. Otte, M. Ternes, C. P. Lutz, B. A. Jones, and A. J. Heinrich, Science **317**, 1199 (2007).
[9] T. Miyamachi, T. Schuh, T. Märkl, C. Bresch, T. Balashov, A. Stöhr, C. Karlewski, S. André, M. Marthaler, M. Hoffmann, M. Geilhufe, S. Ostanin, W. Hergert, I. Mertig, G. Schön, A. Ernst, and W. Wulfhekel, Nature (London) **503**, 242 (2013).
[10] F. Donati, A. Singha, S. Stepanow, C. Wäckerlin, J. Dreiser, P. Gambardella, S. Rusponi, and H. Brune, Phys. Rev. Lett. **113**, 237201 (2014).
[11] C. Karlewski, M. Marthaler, T. Märkl, T. Balashov, W. Wulfhekel, and G. Schön, Phys. Rev. B **91**, 245430 (2015).
[12] C. Hübner, B. Baxevanis, A. A. Khajetoorians, and D. Pfannkuche, Phys. Rev. B **90**, 155134 (2014).
[13] M. Prada (private communication).
[14] M. Andrut, M. Wildner, and C. Rudowicz, in *Spectroscopic Methods in Mineralogy*—European Mineralogical Union Notes in Mineralogy, Vol. 6, edited by A. Beran and E. Libowitzky (Eötvös University Press, Budapest, 2004), pp. 145–188.
[15] Edited by D. J. Newman and B. Ng, *Crystal Field Handbook* (Cambridge University Press, Cambridge, 2000).
[16] J. Mulak and Z. Gajek, *The Effective Crystal Field Potential* (Elsevier, Amsterdam, 2000).
[17] B. G. Wybourne, *Spectroscopic Properties of Rare Earths* (Wiley, New York, 1965).
[18] C. Görller-Walrand and K. Binnemans, in *Handbook on the Physics and Chemistry of Rare Earths*, Vol. 23, edited by K. A. Gschneidner, Jr. and L. Eyring (Elsevier, Amsterdam, 1996), p. 121.
[19] J. A. Weil and J. R. Bolton, *Electron Paramagnetic Resonance, Elemental Theory and Practical Applications* (Wiley, New York, 2007).
[20] F. E. Mabbs and D. Collison, *Electron Paramagnetic Resonance of d Transition-Metal Compounds* (Elsevier, Amsterdam, 1992).
[21] Edited by S. K. Misra, *Multifrequency Electron Paramagnetic Resonance* (Wiley-VCH, Weinheim, 2011).
[22] K. H. J. Buschow and F. R. de Boer, *Physics of Magnetism and Magnetic Materials* (Kluwer Academic, New York, 2003).
[23] R. Boča, Struct. Bond. **117**, 1 (2006).
[24] D. Gatteschi, R. Sessoli, and J. Villain, *Molecular Nanomagnets* (Oxford University Press, Oxford, 2006).
[25] C. Rudowicz and M. Karbowiak, Coord. Chem. Rev. **287**, 28 (2015), and references therein.
[26] C. Rudowicz and M. Karbowiak, Physica B **451**, 134 (2014).
[27] C. Rudowicz and M. Karbowiak, Physica B **456**, 330 (2015).
[28] F. Neese, Coord. Chem. Rev. **253**, 526 (2009).
[29] C. Duboc, M.-N. Collomb, and F. Neese, Appl. Magn. Reson. **37**, 229 (2010).
[30] T. Balashov, T. Miyamachi, T. Schuh, T. Märkl, C. Bresch, and W. Wulfhekel, Surf. Sci. **630**, 331 (2014).
[31] D. Coffey, J. L. Diez-Ferrer, D. Serrate, M. Ciria, C. de la Fuente, and J. I. Arnaudas, Sci. Rep. **5**, 13709 (2015).
[32] M. Karbowiak, C. Rudowicz, and P. Gnutek, Opt. Mater. **33**, 1147 (2011).
[33] C. Rudowicz, M. Chua, and M. F. Reid, Physica B **291**, 327 (2000).
[34] Y. Y. Yeung, M. F. Reid, and D. J. Newman, in *Crystal Field Handbook,* edited by D. J. Newman and B. Ng (Cambridge University Press, Cambridge, 2000), pp. 254–258.
[35] C. Rudowicz, Magn. Res. Rev. **13**, 1 (1987); **13**, 335 (1988).
[36] C. Rudowicz, Chem. Phys. **97**, 43 (1985).
[37] C. Rudowicz, P. Gnutek, and M. Karbowiak, Opt. Mater. **33**, 1557 (2011).
[38] M. Karbowiak, J. Cichos, and C. Rudowicz, J. Phys. Chem. A **116**, 10574 (2012).
[39] M. Karbowiak, P. Gnutek, and C. Rudowicz, Chem. Phys. **400**, 29 (2012).

[40] See Supplemental Material at http://link.aps.org/supplemental/10.1103/PhysRevB.93.184415 for definitions and details of SPM/CFP calculations and analysis of results.
[41] D. J. Newman, J. Phys. F: Met. Phys. **13**, 1511 (1983).
[42] M. Divis, Phys. Status Solidi B **164**, 227 (1991).
[43] C. Rudowicz, J. Phys. C: Solid State Phys. **18**, 1415 (1985); **18**, 3837 (1985).
[44] C. Rudowicz and C. Y. Chung, J. Phys.: Condens. Matter **16**, 5825 (2004).
[45] C. Rudowicz, J. Phys. C: Solid State **20**, 6033 (1987).
[46] D. J. Newman and B. Ng, in *Crystal Field Handbook,* edited by D. J. Newman and B. Ng (Cambridge University Press, Cambridge, 2000), pp. 83–119.
[47] H. Schilder and H. Lueken, J. Magn. Magn. Mater. **281**, 17 (2004).
[48] J. van Leusen, M. Speldrich, H. Schilder, and P. Kögerler, Coord. Chem. Rev. **289-290**, 137 (2015).
[49] N. Ishikawa, Polyhedron **26**, 2147 (2007).
[50] B. S. Tsukerblat, *Group Theory in Chemistry and Spectroscopy* (Academic Press, London, 1994).
[51] M. Steinbrecher, A. Sonntag, M. dos Santos Dias, M. Bouhassoune, S. Lounis, J. Wiebe, R. Wiesendanger, and A. A. Khajetoorians, Nat. Commun. **7**, 10454 (2016).
[52] C. Rudowicz, M. Karbowiak, and K. Tadyszak (unpublished).
[53] C. Rudowicz and K. Tadyszak (unpublished).